

Asymmetry in self-assembled quantum dot-molecules made of identical InAs/GaAs quantum dots

Lixin He, Gabriel Bester, and Alex Zunger

National Renewable Energy Laboratory, Golden, Colorado 80401

(Dated: August 23, 2018)

We show that a diatomic dot molecule made of two identical, vertically stacked, strained InAs/GaAs self-assembled dots exhibits an asymmetry in its single-particle and many-particle wavefunctions. The single-particle wave function is asymmetric due to the inhomogeneous strain, while the asymmetry of the many-particle wavefunctions is caused by the correlation induced localization: the lowest singlet $^1\Sigma_g$ and triplet $^3\Sigma$ states show that the two electrons are each localized on different dots within the molecule, for the next singlet states $^1\Sigma_u$ both electrons are localized on the same (bottom) dot for interdot separation $d > 8$ nm. The singlet-triplet splitting is found to be ~ 0.1 meV at inter-dot separation $d=9$ nm and as large as 100 meV for $d=4$ nm, orders of magnitude larger than the few meV found in the large (50 - 100 nm) electrostatically confined dots.

PACS numbers: 73.63.Kv, 85.35.-p, 73.23.Hk

Quantum dot-molecules (QDM) occupied by two electronic spins have been proposed as a basis for quantum computation.¹ Loss and DiVincenzo² proposed a “swap gate” based on a simplified model in which the two localized spins have Heisenberg coupling $H = J_{S-T} \vec{S}_1 \cdot \vec{S}_2$, where \vec{S}_1 and \vec{S}_2 are the spin- $\frac{1}{2}$ operators for the two localized electrons, and J_{S-T} is the effective Heisenberg exchange splitting, being the difference in energy between the spin-triplet state with total spin $S = 1$ and the spin-singlet with $S = 0$. Successful operation would require a large-singlet triplet splitting J_{S-T} (fast swap time²), and that the probability $Q_{\text{tot}}^{(\nu)}$ of the two electrons in state ν simultaneously occupying one dot be small (maximizing entanglement³). The search for a nanosystem with large J_{S-T} and small $Q_{\text{tot}}^{(\nu)}$ involves engineering of the properties of the corresponding many-particle wave functions. In a simplified molecular model, the single-particle wave functions of the two electrons are given by bonding $\psi_{\sigma_g} = (\chi_T + \chi_B)/\sqrt{2}$ and antibonding $\psi_{\sigma_u} = (\chi_T - \chi_B)/\sqrt{2}$ molecular orbitals, constructed from the individual orbitals χ of the top (T) and bottom (B) dot. The many-particle states are then the corresponding product states $|\sigma_g^{\uparrow}\sigma_g^{\downarrow}\rangle \sim ^1\Sigma_g$ (singlet), and $|\sigma_g^{\uparrow}\sigma_u^{\downarrow}\rangle \sim ^3\Sigma$ (triplet), etc. In this picture both single-particle molecular orbitals and the many-particle states are delocalized on both dots constituting the dot-molecule. Here, we discuss via atomistic single-particle and many-body calculations two important deviations from this simplified molecular picture, leading to asymmetries both in the single-particle molecular orbitals due to the inhomogeneous strains, and in the many-body states (i.e. localization either on T or on B) as a consequence of correlation. For the many-body states we find Mott-like transitions for the first and third singlet states: both electrons are localized on one dot at large d and delocalized over both dots are small d . The double occupancy $Q_{\text{tot}}^{(\nu)}$ of the first singlet state is surprisingly large ($\simeq 40\%$) for an interdot separation of 5 nm. The triplet states and the second singlet state are Mott-localized at

every interdot separations with $Q_{\text{tot}}^{(\nu)}=0$ (no double occupation) for the triplet states and $Q_{\text{tot}}^{(\nu)}=1$ for the singlet state.

Previous models of dot-molecules have focused on electrostatically-confined dots^{4,5,6}, which have a very large confining dimension of 50 - 100 nm. Such dots exhibit typical single-particle level spacings of $\Delta\epsilon_e=3 - 5$ meV, Coulomb energies J_{ee} of about 5 meV $\geq \Delta\epsilon_e$, whereas exchange energies and correlation energies are around 1 meV. Many experiments were recently done on *two* such coupled dots^{7,8}, showing that the splitting between the bonding and anti-bonding molecular levels is as large as 3.5 meV at an interdot separation of 2.5 nm, comparable to the single-particle energy spacing $\Delta\epsilon_e$ of the single dot. Because of the very large size of such dots, their single-particle levels can be described by simple one-band effective mass “particle in a box” models using the external potential generated by a combination of band offset, the gate potential and the ionized impurities.^{9,10} Alternatively, one can simply assume a particle-in-a-parabolic well model.^{11,12} In these descriptions, the single-particle states are symmetric, but many-electron symmetry breaking is possible due to correlation effects, as shown via unrestricted Hartree-Fock treatment of the effective-mass approximation (UHF-EMA),¹³, configuration-interaction treatment of the effective-mass approximation (CI-EMA),¹² or Mott-Hubbard model.¹⁴

Here, we discuss localization effects and singlet-triplet splitting of electrons in vertically coupled self-assembled InAs/GaAs quantum dot molecules grown epitaxially^{15,16,17}. Such dots have much smaller confining dimensions (height of 3 - 5 nm), and when made of InAs/GaAs their electronic level splitting is $\Delta\epsilon_e \sim 40 - 50$ meV, *larger* than the interelectronic Coulomb repulsion $J_{ee} \sim 10 - 20$ meV, and the exchange energy $K_{ee} \sim 2 - 5$ meV. In this paper, we show that in vertically aligned self-assembled dots, one can achieve singlet-triplet splittings of up to 100 meV.

Figure 1a shows the geometry selected for the dot

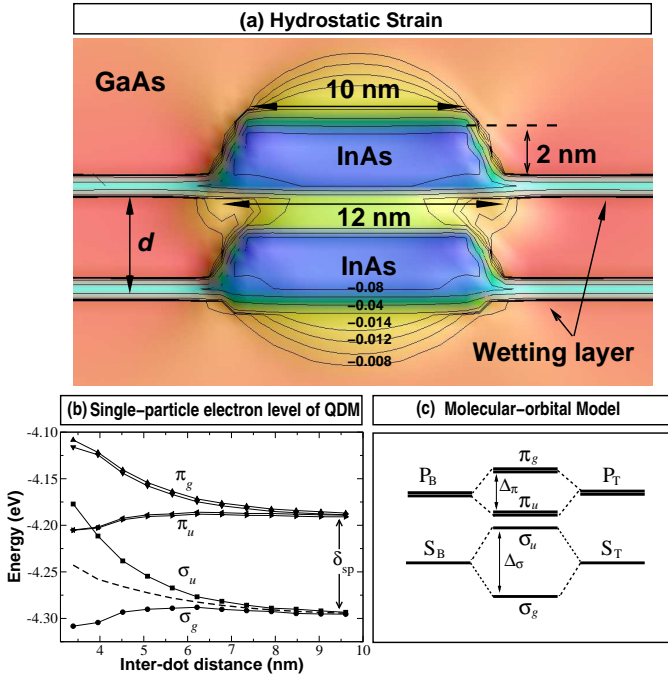


FIG. 1: (a) (Color online) Contour plot of the hydrostatic strain $\text{Tr}(\epsilon)$ in the two vertically coupled quantum dots. The inter-dot distance d is measured from one wetting layer to the next. The iso-strain values are also marked in the figure. (b) Molecular orbital energy levels vs. inter-dot distance. The dashed line is the average of σ_g and σ_u . δ_{sp} is the single dot s-p energy level splitting. (c) Sketch of bonding-antibonding splitting. S_T , S_B are “s” while P_T and P_B are “p” single dot orbitals on top and bottom dots. Here $S_T + S_B = \sigma_g$ and $P_T + P_B = \pi_u$ are bonding states, while the $S_T - S_B = \sigma_u$ and $P_T - P_B = \pi_g$ are antibonding states.

molecules, consisting of two-dimensional InAs wetting layers, a pair of 2 nm tall InAs dots in the shape of truncated cones embedded in a GaAs matrix. The considered dots are identical and describe the experimental extreme case of perfect growth. In reality, both dots can be geometrically and compositionally different. This extrinsic inequivalence would reinforce the intrinsic asymmetry of the system which our results describe. The hydrostatic strain field $\text{Tr}(\epsilon)$, with the iso-strain lines shown in Fig. 1a, is calculated atomistically by relaxing the bond-stretching and bond-bending forces according to the valence force field model (VFF).^{18,19} It is clearly seen in Fig. 1a that both dots have large and nearly constant hydrostatic strain inside the dots which decays rapidly outside the dots. However, even though the dots comprising the molecule are the same, the strain on the two dots is different since the molecule lacks inversion symmetry. We see that the top dot is slightly more strained than the bottom dot. Furthermore, the GaAs region between the two dots is much more strained than in other parts of the matrix.

Having established a realistic geometry and the relaxed atomic positions $\{\mathbf{R}_{m,\alpha}\}$, we calculate the single-

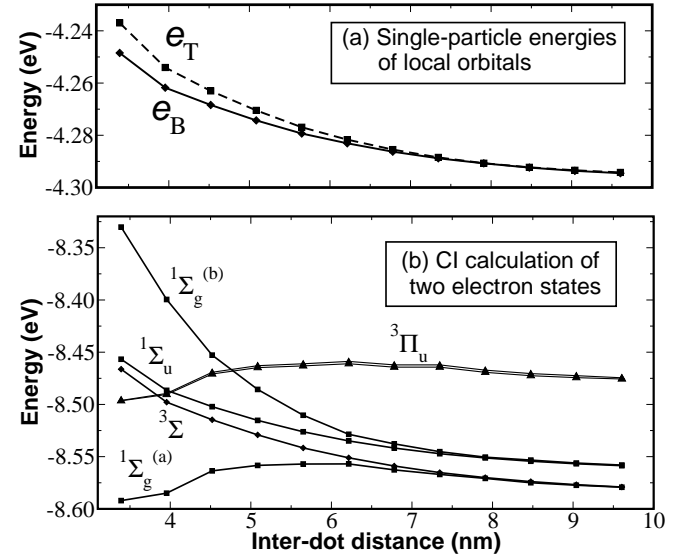


FIG. 2: (a) The effective single-particle energy levels e_T and e_B of dot-centered orbitals on the top dot and bottom dot respectively. (b) Energy of two-electron states calculated from CI using all confined molecular orbitals.

particle electronic structure by constructing a pseudopotential $V(\mathbf{r}) = \sum_{m,\alpha} v_\alpha(\mathbf{r} - \mathbf{R}_{m,\alpha})$ from a superposition of screened atomic potentials v_α of species $\alpha = \text{Ga, In, As}$. Here, v_α is constructed²⁰ by fitting to available experimental data the bulk InAs and GaAs band energies, effective-masses, hydrostatic and biaxial deformation potentials, and band-offsets. The pseudopotentials used in present work are taken from Ref. 20. The Schrödinger equation is solved by the Linear Combination of Bulk Bands (LCBB)²¹ method in a basis $\{\phi_{n,\mathbf{k},\vec{\epsilon}}^{(\lambda)}(\mathbf{r})\}$ of Bloch orbitals, i.e. $\psi_i(\mathbf{r}) = \sum_{n,\mathbf{k},\lambda} C_{n,\mathbf{k},\lambda}^{(i)} \phi_{n,\mathbf{k},\vec{\epsilon}}^{(\lambda)}(\mathbf{r})$ of band index n and wave vector \mathbf{k} of material λ ($= \text{InAs, GaAs}$). The basis functions are strained uniformly to constant but different strains $\vec{\epsilon}$. We use $\vec{\epsilon} = 0$ for the (unstrained) GaAs matrix material, and an average $\vec{\epsilon}$ value from VFF for the strained dot material (InAs). For the InAs/GaAs system, we use $n = 2$ for electron states on a $6 \times 6 \times 28$ k-mesh. Unlike the effective-mass description of single-particle state used for electrostatic dot,^{9,10,11,12} here we allow inter-band and inter-valley coupling.

Asymmetry of single-particle states: Figure 1b shows the single-particle dot-molecule energy levels as a function of inter-dot distance d . These results can be generally understood using bonding/antibonding molecular orbitals as shown in Fig. 1c. At large d , the energy levels converge to those of single dots, showing an s-level and, at $\delta_{sp} = 106$ meV higher, two p-levels split by a few meV reflecting the atomistic C_{2v} symmetry of the cylindrically symmetric dots²². Bonding and antibonding molecular orbitals form when the two dots interact: the two single-dot s orbitals form molecular σ_g and σ_u orbitals, whereas the four single-dot p orbitals (two on

each dot) form two molecular π_u and two molecular π_g orbitals.¹² Note that the splitting of σ_g from σ_u is not symmetric, as can be seen by looking at the average of both energies in Fig. 1b (dashed line). The average energy increases with decreasing interdot separation in response to the strain exerted by the presence of the other dot (Fig.1a). Beyond this overall effect, the strain field is different on both geometrically identical dots because the dots are non-spherical (Fig.1a) and lack inversion symmetry. This causes an asymmetry of the molecular orbitals at short interdot distances. At $d \sim 3.4$ nm, we found that the bonding (anti-bonding) states are slightly more localized on the bottom (top) dot. In previous effective-mass calculations,^{7,8,11,12,13} strain effects were not included and single-particle asymmetry was not found. Particularly, in Ref.7, an *ad hoc* parameter was introduced to force the asymmetry of the dot molecule.

A more quantitative analysis of the asymmetry can be given when the molecular orbitals are transformed via a Wannier-like transformation into single dot states. These can be obtained from a unitary rotation of *molecular* orbitals ψ_i ,

$$\chi_{l,p} = \sum_i \mathcal{U}_{l,p}^{(i)} \psi_i, \quad (1)$$

where, ψ_i is the i -the molecular orbital and $\chi_{l,p}$ are the rotated, dot-centered orbitals (the l -th orbital localized on p = T or B dot). \mathcal{U} are unitary matrices, $\mathcal{U}^\dagger \mathcal{U} = I$, chosen to maximize the total self-Coulomb energy.^{23,24} Once $\mathcal{U}_{l,p}^{(i)}$ are known, we define the orbital energies of the dot-centered states $\chi_{l,p}$ as:

$$e_{l,p} = \langle \chi_{l,p} | \hat{T} | \chi_{l,p} \rangle = \sum_i (\mathcal{U}_{l,p}^{(i)})^* \mathcal{U}_{l,p}^{(i)} \epsilon_i, \quad (2)$$

where \hat{T} is the kinetic energy operator, and ϵ_i is the energy of the i -th molecular orbital. The energies $e_{l,p}$ of the dot-centered orbitals are depicted in Fig. 2a as a function of the interdot separation. We see that the single-particle energies for both B and T orbitals rise quickly as the inter-dot distance is reduced, but the energy of the top dot orbital raises faster. At $d \sim 3.4$ nm, there is an energy splitting of ~ 12 meV between top and bottom dot orbitals, which causes the asymmetry of the wave functions between top and bottom dots.

Many-particle symmetry-breaking: Having obtained the “molecular”, single-particle energy (Fig. 1b), and wave functions, we calculate all interelectronic Coulomb and exchange integrals J and K of ψ_i by numerical integration²⁵, and set up a screened configuration-interaction expansion²⁶. A microscopic position-dependent dielectric screening²⁶ is applied to both Coulomb and exchange integrals to represent the inner electrons that are not calculated explicitly. Considering six molecular orbitals σ_g , σ_u , π_u , π_g of Fig. 1b, we have a total of 66 Slater determinants. The many-body wave functions Ψ_ν are written as linear combinations of these

determinants $|\Phi_{\mathcal{C}}\rangle$ as, $\Psi_\nu = \sum_{\mathcal{C}} A_\nu(\mathcal{C}) |\Phi_{\mathcal{C}}\rangle$. The resulting many-particle energies are shown as a function of interdot separation in Fig. 2b. The energy splittings J_{S-T} between the ground state singlet $^1\Sigma_g^{(a)}$ and triplet $^3\Sigma$ ranges from 0 - 100 meV and is much larger than in electrostatic dot molecules (< 1 meV).^{4,5,6} In Fig.3a we decompose the two-electron wave functions into the leading configurations $\Phi_1 = |\sigma_g^\uparrow \sigma_u^\downarrow\rangle$, $\Phi_2 = |\sigma_g^\downarrow \sigma_u^\uparrow\rangle$, $\Phi_3 = |\sigma_g^\uparrow \sigma_g^\downarrow\rangle$, and $\Phi_4 = |\sigma_u^\uparrow \sigma_u^\downarrow\rangle$. The ground state is the singlet $^1\Sigma_g^{(a)}$ state, followed by the three-fold degenerated triplet states $^3\Sigma$ (we depict only the $s_z=0$ state made of $\Phi_1 + \Phi_2$ in Fig.3) and the next singlets $^1\Sigma_u$ (made of $\Phi_1 - \Phi_2$) and $^1\Sigma_g^{(b)}$. To explore the localization of these states, we plot in Fig.3b and 3c, the pair correlation functions $P_\nu(\mathbf{r}_0, \mathbf{r}) = |\Psi_\nu((\mathbf{r}_0, \mathbf{r})|^2$ where \mathbf{r}_0 is fixed at the center of the bottom dot. $P_\nu(\mathbf{r}_0, \mathbf{r})$ gives the probability of finding the second electron at position \mathbf{r} given that the first electron has been found at \mathbf{r}_0 . For the ground state singlet $^1\Sigma_g^{(a)}$, we see that at the small interdot separation $d=4$ nm, the probability to find the second electron in the top or the bottom dot are comparable, suggesting a molecular-like delocalized state. Accordingly, the wave function analysis reveals a dominant contribution from the product of two delocalized molecular orbitals Φ_3 . With increasing interdot separation, the electrons show correlation induced (i.e. the coupling between Φ_3 and Φ_4) localization. At $d=7$ nm, the second electron is almost entirely localized on the top dot as shown in Fig. 3c. A similar delocalized to localized transition applies for the $^1\Sigma_g^{(b)}$ state, with the difference, that at large d both electrons are localized on the same (bottom) dot. In contrast, the triplet states $^3\Sigma$ and the singlet $^1\Sigma_u$ show localization at all interdot distances. However, for the triplet states the two electrons are localized on different dots while for $^1\Sigma_u$ both electrons are localized on the same dot.

To understand the (hidden) broken-symmetry (i.e. the wave function localization) in the many-particle CI wave functions, and to study the degree of localization quantitatively, we resort to the Wannier-like transformation of Eq. (1). The CI matrix elements expressed initially in the molecular basis ψ_i [Eq. (1)] are transformed into the dot-centered Wannier basis $\chi_{l,p}$ [Eq. (1)]. For example, $\{|\chi_{l,p}^\sigma, \chi_{l',p'}^{\sigma'}\rangle\}$ denotes the configuration where one electron is on the l -th orbital of the p dot with spin σ , and the other electron is on the l' -th orbital of the p' dot with spin σ' . The two electrons can be either both on the top dots, or both on the bottom dots, or one on the top and the other on the bottom dots. We can thus define a “bi-electron localization parameter” $Q_{pp}^{(\nu)}$ as the probability of two electrons occupying the dot p = (T or B) at the same time in the many-particle state ν ,

$$Q_{pp}^{(\nu)} = \sum_{l\sigma, l'\sigma'} P_\nu(|\chi_{l,p}^\sigma, \chi_{l',p'}^{\sigma'}\rangle), \quad (3)$$

where $P_\nu(\mathcal{C})$ is the weight of the configuration \mathcal{C} in the many-body wave functions of state ν . The total prob-

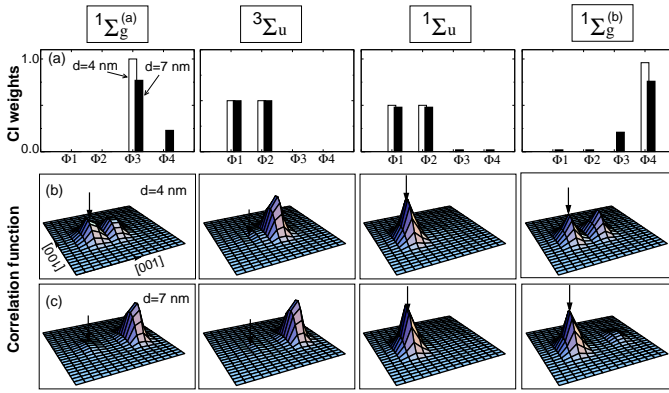


FIG. 3: (Color online) Panel (a) gives the weights of configurations Φ_1 , Φ_2 , Φ_3 and Φ_4 of the many-particle CI wave functions. Panels (b) and (c) depict the probability of finding the second electron at position \mathbf{r} given that the first electron has been found on the center of the bottom dot (indicated by the arrows) for the interdot distances (b) $d=4$ nm and (c) $d=7$ nm.

ability of two electrons being on the *same* dot is then $Q_{\text{tot}}^{(\nu)} = Q_{\text{TT}}^{(\nu)} + Q_{\text{BB}}^{(\nu)}$ for the ν -th state. Figure 4, shows the bielectron localization parameter $Q_{pp}^{(\nu)}$ of Eq.(3) for the many-particle states $\nu = 1\Sigma_g$, $1\Sigma_u$. We see that: (i) For the ground state $1\Sigma_g^{(a)}$ (Fig. 4a), $Q_{\text{BB}} > Q_{\text{TT}}$ at all inter-dot separations (as is the case for the $1\Sigma_u$ state), whereas for state $1\Sigma_g^{(b)}$ (Fig. 4c), we always have $Q_{\text{TT}} > Q_{\text{BB}}$, indicating symmetry breaking for these many-body wave functions. (ii) The ground state $1\Sigma_g^{(a)}$ has a very small Q_{pp} at large inter-dot separation ($d > 8$ nm), whereas for $1\Sigma_g^{(b)}$, the probability of two electrons being on the same dot is close to 1. At smaller d , Q_{tot} increases rapidly for $1\Sigma_g^{(a)}$, while it decreases for $1\Sigma_g^{(b)}$. (iii) Our calculations show that the coupling between $^3\Sigma$ and higher triplet configurations is negligible, thus the calculated $Q_{pp}(^3\Sigma)$ are zero (not shown), i.e. the electrons are on different dots, due to the Pauli principle. However, in large electrostatic quantum dot molecules^{4,5,6} (with $J_{ee} > \Delta\epsilon_e$), where the lowest $^3\Sigma$ state is expected to mix with higher energy triplet configurations and acquire non-zero double electron occupations, $Q_{pp}^{(\nu)} > 0$. (iv) $Q_{\text{tot}}(1\Sigma_u)$ is close to 1 for all inter-dot distances (Fig. 4b) and both electrons are therefore occupying the same dots.

As we have noted in the introduction, quantum computing based on two spins in dot molecules requires that (i) $Q_{\text{tot}}^{(\nu)} \ll 1$ i.e. the electrons should be localized on different dots as much as possible. We now see this is satisfied for $^3\Sigma_u$, but not for the singlets $1\Sigma_u$ and $1\Sigma_g^{(b)}$. For $1\Sigma_g^{(a)}$, we find $Q_{\text{tot}}^{(\nu)} \ll 1$ only at large inter-dot separation d . (ii) Two spins should have high entanglement. Since entanglement is maximized for pure singlet and triplet states without double-occupancy (i.e. $Q_{\text{tot}}=0$), this also requires that $Q_{\text{tot}}^{(\nu)} \ll 1$. (iii) The inter-dot separation should be such that significant singlet-triplet split-

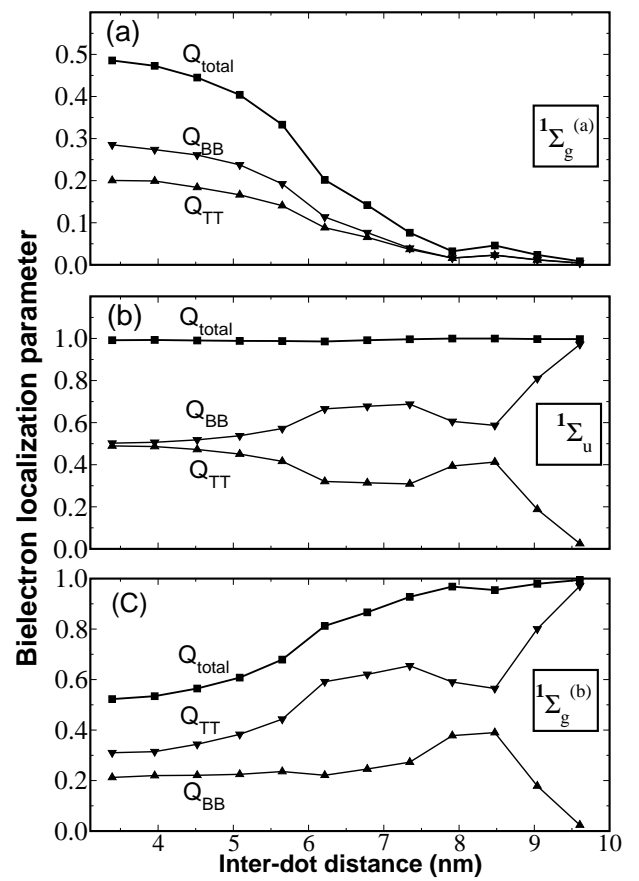


FIG. 4: The probability of two electrons occupying the same dot [Eq.(3)] for (a) $1\Sigma_g^{(a)}$, (b) $1\Sigma_u$, (c) $1\Sigma_g^{(b)}$ states. Q_{TT} (Q_{BB}) is the probability of both electrons being on the top (bottom) dot, while Q_{total} gives the total probability.

ting exist. Conditions (i) and (ii) require large inter-dot separation d , while (iii) requires small d . Considering all the present results, the requirements for quantum computation are best met for the ground state $1\Sigma_g^{(a)}$ at an inter-dot distance of 6 to 8 nm, where we have significant J_{S-T} , and Q_{tot} is small.

To conclude, we investigated the wave function asymmetry of both single-particle and many-particle wave functions in the quantum dot-molecules made of two identical, vertically stacked InAs/GaAs self-assembled quantum dots. For single-particle states, we find the asymmetry at short interdot separations introduced by the inhomogeneous strains. For many-particle states, we find that two electrons are always on different dots in the triplet state, while for the ground state singlet, the probability of ‘bielectron localization’ is not zero and increases rapidly as the two dots come close to each other. The ideal interdot separation where the two electron spins can be used for quantum information is around 6 -8 nm. At this distance the singlet-triplet splitting is large but the double electron occupation still low.

This work was supported by US DOE-SC-BES-DMS,

grant no. DEAC36-98-GO10337.

¹ D. P. DiVincenzo, *Science* **270**, 255 (1995).

² D. Loss and D. P. DiVincenzo, *Phys. Rev. A* **57**, 120 (1998).

³ J. Schliemann, D. Loss, and A. H. MacDonald, *Phys. Rev. B* **63**, 085311 (2001).

⁴ R. C. Ashoori, H. L. Stormer, J. S. Weiner, L. N. Pfeiffer, S. J. Pearton, K. W. Baldwin, and K. W. West, *Phys. Rev. Lett.* **68**, 3088 (1992).

⁵ A. T. Johnson, L. P. Kouwenhoven, W. de Jong, N. C. van der Vaart, C. J. P. M. Harmans, and C. T. Foxon, *Phys. Rev. Lett.* **69**, 1592 (1992).

⁶ S. Tarucha, D. G. Austing, T. Honda, R. J. van der Hage, and L. P. Kouwenhoven, *Phys. Rev. Lett.* **77**, 3613 (1996).

⁷ M. Pi, A. Emperador, M. Barranco, F. Garcias, K. Muraki, S. Tarucha, and D. G. Austing, *Phys. Rev. Lett.* **87**, 066801 (2001).

⁸ M. Rontani, S. Amaha, K. Muraki, F. Manghi, E. Molinari, S. Tarucha, and D. G. Austing, *Phys. Rev. B* **69**, 085327 (2004).

⁹ L. R. C. Fonseca, J. L. Jimenez, J. P. Leburton, and R. M. Martin, *Phys. Rev. B* **57**, 4017 (1998).

¹⁰ S. Bednarek, B. Szafran, K. Lis, and J. Adamowski, *Phys. Rev. B* **68**, 155333 (2003).

¹¹ X. Hu and S. DasSarma, *Phys. Rev. A* **61**, 62301 (2000).

¹² M. Rontani, F. Troiani, U. Hohenester, and E. Molinari, *Solid State Comm.* **119**, 309 (2001).

¹³ C. Yannouleas and U. Landman, *Phys. Rev. Lett.* **82**, 5325 (1999).

¹⁴ C. A. Stafford and S. D. Sarma, *Phys. Rev. Lett.* **72**, 3590 (1994).

¹⁵ D. Bimberg, M. Grundmann, and N. N. Ledentsov, *Quantum Dot Heterostructures* (John Wiley & Sons, 1999).

¹⁶ T. Ota, M. Stopa, M. Rontani, T. Hatano, K. Yamada, S. Tarucha, H. Song, Y. Nakata, T. Miyazawa, T. Ohshima, et al., *Superlattices and Microstructures* **34**, 159 (2003).

¹⁷ T. Ota, K. Ono, M. Stopa, T. Hatano, S. Tarucha, H. Z. Song, Y. Nakata, T. Miyazawa, T. Ohshima, and N. Yokoyama, *Phys. Rev. Lett.* **93**, 66801 (2004).

¹⁸ P. N. Keating, *Phys. Rev.* **145**, 637 (1966).

¹⁹ J. L. Martins and A. Zunger, *Phys. Rev. B* **30**, R6217 (1984).

²⁰ A. J. Williamson, L.-W. Wang, and A. Zunger, *Phys. Rev. B* **62**, 12963 (2000).

²¹ L.-W. Wang and A. Zunger, *Phys. Rev. B* **59**, 15806 (1999).

²² G. Bester and A. Zunger, *Phys. Rev. B* **71**, 045318 (2005).

²³ C. Edmiston and K. Ruedenberg, *Rev. Mod. Phys.* **35**, 457 (1963).

²⁴ L. He, G. Bester, and A. Zunger, to be published.

²⁵ A. Franceschetti and A. Zunger, *Phys. Rev. Lett.* **78**, 915 (1997).

²⁶ A. Franceschetti, H. Fu, L.-W. Wang, and A. Zunger, *Phys. Rev. B* **60**, 1819 (1999).